



OPEN ACCESS

EDITED BY

Miao Li,
Charles Sturt University, Australia

REVIEWED BY

Shuai Cao,
University of Science and Technology
Beijing, China
Yue Xiao,
Wuhan University of Technology, China

*CORRESPONDENCE

Changlong Wang,
✉ baistuwong@139.com

RECEIVED 29 April 2023

ACCEPTED 10 July 2023

PUBLISHED 20 July 2023

CITATION

Yuan D, Liang X, Gao Y, Ping H, Wang C,
Ma J, Zheng Y, Jing J, Qi Y, Zhai Y and
Liu F (2023), High-temperature
modification of steel slag using
composite modifier containing silicon
calcium slag, fly ash, and
reservoir sediment.
Front. Earth Sci. 11:1214182.
doi: 10.3389/feart.2023.1214182

COPYRIGHT

© 2023 Yuan, Liang, Gao, Ping, Wang, Ma,
Zheng, Jing, Qi, Zhai and Liu. This is an
open-access article distributed under the
terms of the [Creative Commons
Attribution License \(CC BY\)](https://creativecommons.org/licenses/by/4.0/). The use,
distribution or reproduction in other
forums is permitted, provided the original
author(s) and the copyright owner(s) are
credited and that the original publication
in this journal is cited, in accordance with
accepted academic practice. No use,
distribution or reproduction is permitted
which does not comply with these terms.

High-temperature modification of steel slag using composite modifier containing silicon calcium slag, fly ash, and reservoir sediment

Dongxia Yuan¹, Xiaoying Liang¹, Ying Gao¹, Haoyan Ping¹,
Changlong Wang^{1*}, Jintao Ma¹, Yongchao Zheng², Jianlin Jing¹,
Yang Qi², Yuxin Zhai³ and Feng Liu⁴

¹Collaborative Innovation Center for Intelligent Regulation and Integrated Management of Water Resources Jointly Built by Provinces and Ministries, School of Civil Engineering, Hebei University of Engineering, Handan, China, ²State Key Laboratory of Solid Waste Reuse for Building Materials, Beijing Building Materials Academy of Science Research, Beijing, China, ³China Railway Construction Group Co., LTD., Beijing, China, ⁴China Railway Construction Group Construction Development Co., Ltd., Beijing, China

Steel slag (SS) is a kind of industrial solid waste, and its accumulation brings certain harm to the ecological environment. In order to promote the building material utilization of SS, high-temperature modification (HTM) of SS is performed using a composite modifier (CMSFR) containing silicon calcium slag (SCS), fly ash (FA), and reservoir sediment (RS). Then, the authors investigated the effect of CMSFR on the cementitious properties and volume soundness of SS mixture after HTM (SMHTM). After that, the mineral composition and microstructure of SMHTM were investigated through X-ray fluorescence analysis (XRF), X-ray diffraction (XRD), scanning electronic microscopy (SEM), energy dispersive spectrometry (EDS), and particle size analysis. It was found that the free CaO (f-CaO) content obviously decreased, and the cementitious properties improved in SMHTM. When the CMSFR content was 20% (SCS: FA: RS = 9:7:4), and the modification temperature (MT) was 1,250°C, the mass fraction of f-CaO in SMHTM dropped from 4.81% to 1.90%, down by 60.5%; the 28-day activity index of SMHTM increased to 85.4%, 14.3% higher than that of raw SS, which meets the technical requirement of Steel slag powder used for cement and concrete (GB/T 20491-2017): the activity index of grade I SS powder must be greater than or equal to 80%. As the mass fraction of CMSFR grew from 10% to 30%, new mineral phases formed in SMHTM, including diopside (CMS₂), ceylonite (MgFe₂O₄), gehlenite (C₂AS), tricalcium aluminate (C₃A), and magnetite (Fe₃O₄). The HTM with CMSFR promotes the decomposition of RO phase (a continuous solid solution composed of divalent metal oxides like FeO, MgO, MnO, and CaO) in raw SS, turning the FeO in that phase into Fe₃O₄. The above results indicate that the SMHTM mixed with CMSFR can be applied harmless in cement and concrete, making low-energy fine grinding of SS a possibility.

KEYWORDS

Steel slag (SS), composite modifier, high-temperature modification (HTM), free CaO (f-CaO), cementitious activity

1 Introduction

In order to promote the building material utilization of steel slag (SS), high-temperature modification (HTM) was studied to overcome the shortcomings of low cementitious activity and poor volume soundness of SS, providing reference for the design and production of high-performance SS based cementitious materials. SS is a waste product generated by steel-making industry. Typical SS consists of slag-making materials such as smelting fluxes like limestone, dolomite, and iron ore. These materials are added to modify the properties of steel, as well as the impurities separated from two mutually non-fusing liquid phase furnace materials melted at high temperature. The SS emission is roughly 12–20% of crude steel output (Shi, 2004; Guo et al., 2009; Dhoble and Ahmed, 2018). In China, the annual production of SS is about 80 million tons, and the cumulative storage amounts to around 500 million tons. However, fewer than 30% of SS has been utilized comprehensively (Alanyali et al., 2009; Li et al., 2011; Wang et al., 2018). The accumulation of huge amount of SS pollutes the environment, occupies wide stretches of land, and seriously wastes resources. SS contains some cementitious minerals, it can be used as some raw materials for cement concrete; In addition, there is also a high content of FeO and a certain amount of free CaO (f-CaO) and free MgO (f-MgO) in the SS. FeO cannot be directly separated through magnetic separation and easy to cause SS cement strength reduction. The presence of f-CaO and f-MgO makes the SS difficult to be used as a building materials due to its poor soundness. Thus, the main problems of SS in the process of building materials application can be summarized as the following four aspects: 1) The proportion of iron oxides is large and difficult to separate; 2) Lack of active mineral phase and poor hydration activity; 3) The content of free calcium oxide and magnesium oxide is high, and

their stability is poor; 4) It cannot be mixed into cement in a larger proportion for application.

In terms of chemical composition, SS mainly consists of SiO_2 , CaO, MgO, and Fe_2O_3 , plus a small amount of Al_2O_3 , MnO, and P_2O_5 (Figure 1) (Shi, 2002; Peng and Huang, 2010; Roslan et al., 2016). The main minerals in SS include C_2S ($2\text{CaO}\cdot\text{SiO}_2$), C_3S ($3\text{CaO}\cdot\text{SiO}_2$), C_4AF ($4\text{CaO}\cdot\text{Al}_2\text{O}_3\cdot\text{Fe}_2\text{O}_3$), C_2F ($2\text{CaO}\cdot\text{Fe}_2\text{O}_3$), C_{12}A_7 ($12\text{CaO}\cdot 7\text{Al}_2\text{O}_3$), C_3A ($3\text{CaO}\cdot\text{Al}_2\text{O}_3$), RO phase (a continuous solid solution composed of divalent metal oxides like FeO, MgO, MnO, and CaO), Fe, $\text{Fe}_2\text{O}_3\cdot\text{SiO}_2$, Fe_3O_4 , and f-CaO (Waligora et al., 2010; Liu et al., 2014; Yan et al., 2014; Yüksel, 2017; Humbert and Castro-Gomes, 2019; Liu W. H. et al., 2020). Overall, the chemical and mineral compositions of SS are similar to those of cement. At present, SS is mainly utilized in subgrade engineering (Aldeeky and Hattamleh, 2017; Gu et al., 2018; Wang et al., 2020), mine filling (Li et al., 2021; Zhang et al., 2021; Zhao D. Q. et al., 2022), and asphalt concrete aggregate production (Hasita et al., 2020a; Hasita et al., 2020b; Jiao et al., 2020). The C_2S and C_3S in SS can react with water to generate many hydration products, such as $\text{Ca}(\text{OH})_2$, C-S-A-H gel ($\text{CaO}\cdot\text{Al}_2\text{O}_3\cdot 4\text{SiO}_2\cdot 5\text{H}_2\text{O}$), C-A-H crystal ($\text{CaO}\cdot\text{Al}_2\text{O}_3\cdot 10\text{H}_2\text{O}$), and C-S-H gel ($3\text{CaO}\cdot 2\text{SiO}_2\cdot 3\text{H}_2\text{O}$). Therefore, SS provides a promising auxiliary cementitious material, which could reduce resource waste and protect the environment (Palankar et al., 2016; Mo et al., 2017; Zhuang and Wang, 2021).

Many researchers have explored the potential of SS as an auxiliary cementitious material. Luxán et al. (2020), Li et al. (2011), and Shi (2004) investigated the mineralogical features and microstructure of SS. Qian et al. (2002), Natali Murri et al. (2013), Kriskova et al. (2012), and Wang et al. (2011) modified the hydraulic activity of SS by various means, such as changing the mineral compositions, water quenching, autoclave treatment, and long-

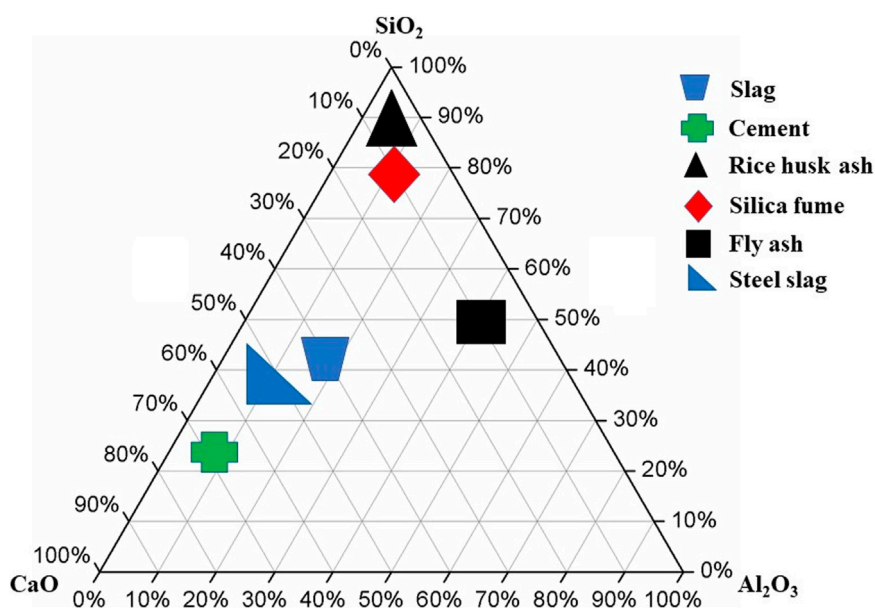


FIGURE 1
Chemical compositions of SS (Shi, 2002).

time milling in ethanol suspension. Additionally, some researchers tried to prepare composite cementitious materials out of SS and cement. These studies have primarily examined the physical and mechanical properties (Monshi and Asgarani, 1999; Shi and Hu, 2003; Adolfsson et al., 2011; Mo et al., 2016), volume expansion (Kourounis et al., 2007), volume soundness (Xue et al., 2006; Anastasiou et al., 2014; Khan et al., 2016; Wang et al., 2017; Saly et al., 2018; Saxena and Tembhurkar, 2018), durability and transportation properties (permeability to chloride ions, and resistance to sulfate attack) (Wang et al., 2013), microstructure (Zhang et al., 2011; Iacobescu et al., 2015; Dai et al., 2022), and hydration products (Zhang et al., 2011; Iacobescu et al., 2015; Rashad, 2019; Dai et al., 2022).

Despite its cementitious properties, SS has not been widely added to cement as an auxiliary cementitious material (Liu J. Z. et al., 2020). The main reasons for the limited application include the soundness problem (the presence of f-CaO and f-MgO in SS may cause volume expansion) (Kourounis et al., 2007; Wu et al., 2007; Guo et al., 2009), poor grindability (RO phase exists in SS), and heavy metal leaching (the presence of Pb, Ba, Cd, Cr, Zn, As, Ni and V) (Tossavainen et al., 2007; Guo et al., 2009; Li et al., 2011; Zhang et al., 2011). SS contains 5%–10% f-CaO, which features high formation temperature, intact crystallization, and solid fusion of some impurities. It takes a long time for f-CaO to complete hydration. Through the reaction of water, the volume of f-CaO would expand by 97.8%. That is why SS has a poor volume soundness (Zhang et al., 2012; Biskri et al., 2017; Tu et al., 2019). What is worse, SS has a content of C₂S and C₃S, only 50%–70% of that in cement clinker (CC). Because of the excessively high formation temperature, the mineral phases form dense and large crystals, which weaken the cementitious performance (Kourounis et al., 2007; Cao et al., 2019; Zhao Y. L. et al., 2022).

In order to promote the application of SS in cement and concrete (Li et al., 2011), several backend modification techniques have been developed to improve its cementitious properties and address the soundness issue. These modification techniques include mechanical activation (Guo and Pan, 2018; Wang et al., 2018; Wang et al., 2019; Guo and Xiong, 2020), thermal activation (Li et al., 2011; Kriskova et al., 2013; Li et al., 2019), and chemical activation (Salman et al., 2015; Huo et al., 2020; Huo et al., 2021). However, these technologies usually require additional energy and chemical activators, and their modification effect varies with the chemical and mineral components of SS. SS is different from Portland CC, granulated blast furnace slag (GBFS) and pozzolanic materials, but its mineral composition is more similar to CC. The direction of modified SS mixture (MSM) can be close to CC, GBFS and pozzolanic materials. However, the potential hydraulic properties of GBFS is mainly related to the large amount of vitreous bodies formed by water quenching of GBFS and the easy dissolution of the fractal structure in an alkaline environment, while MSM cannot obtain a large amount of glass body with the actual cooling method of SS (such as hot splashing method, hot sealing method, etc.) even though its chemical composition is close to that of GBFS. The potential hydraulic hardness of pozzolanic materials is mainly related to their active amorphous substances and spherical aluminum silicate glass bodies, while high-temperature molten SS contains more iron and has a high density, which limits its ability to obtain pozzolanic activity; The hydraulic properties of CC mainly come

from about 75% of the total silicate minerals, which seems to be easier to achieve from the cooling mode and mineral composition of SS. It can be seen from the formation process of SS that the heat enthalpy of liquid SS discharged during converter steelmaking reaches 1,670 MJ·t⁻¹. If the waste heat can be fully utilized to MSM, a large amount of waste heat can be recovered, the composition of SS can be stabilized, and the hydration activity of SS can be improved, realize the purpose of energy saving and waste utilization. Some researchers have experimented with the addition of conditioning components to the steelmaking process in the converter to reform the SS close to the CC at the time of discharge, but due to the high requirements of the steelmaking process on the composition control of the slag and finished steel, the impact on the quality of the molten steel is not allowed, so the feasibility of in-furnace reforming is not strong, and it is easier to achieve high-temperature reforming by mixing the conditioning components at the time of discharge. The method of SS mixture after high-temperature modification (SMHTM) is easier to achieve.

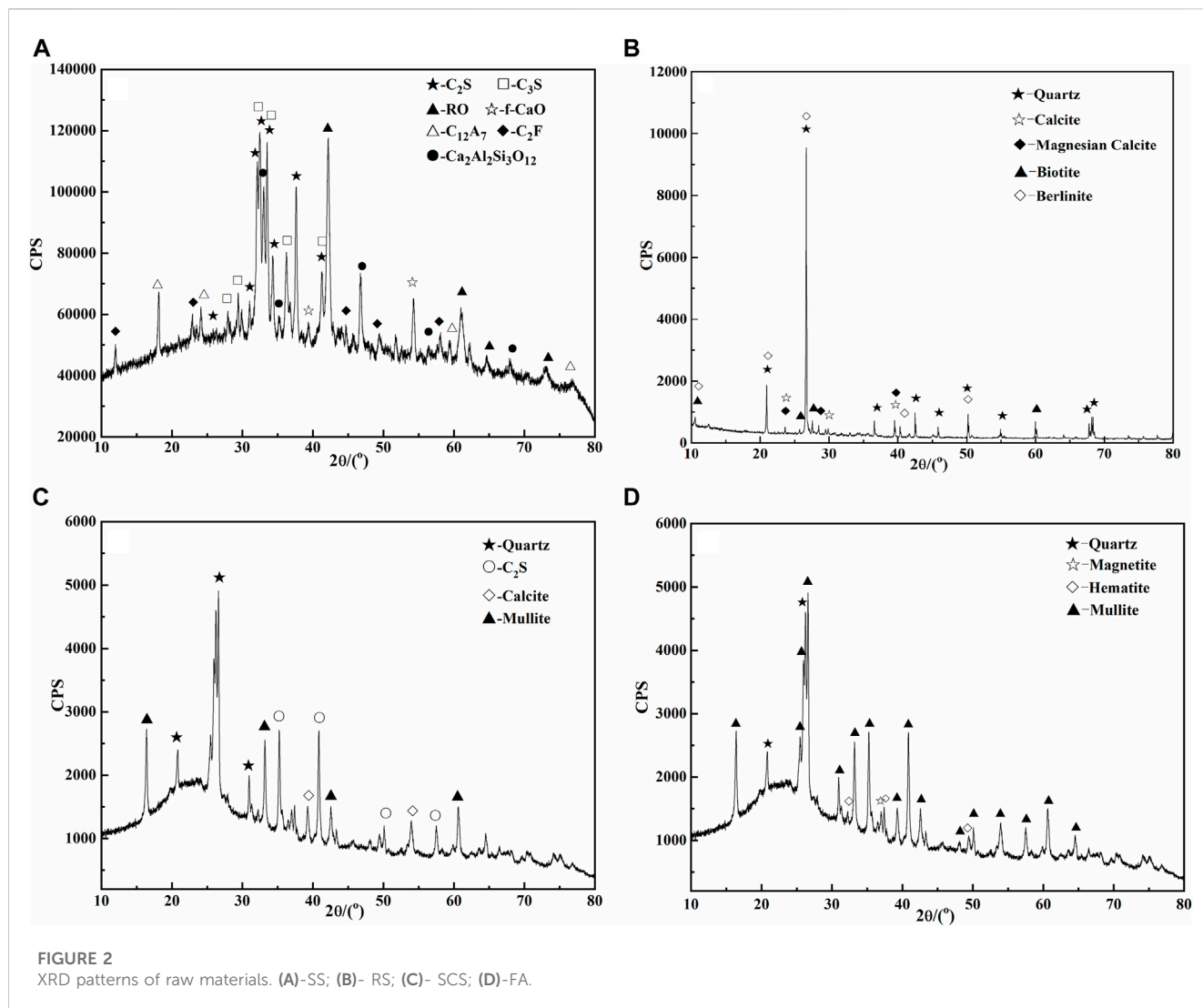
In this study, the authors simulate the on-line MSM outside the furnace. The regulating direction is CC, and the regulating components are silica-alumina and calcium materials, from the perspective of resource conservation and development of green building materials, following the goal of “treating waste with waste”. This study choose reservoir sediment (RS), fly ash (FA), and silicon calcium slag (SCS) to form a composite modifier (CMSFR), and the three wastes corresponding to the adjustment of Si, Al and Ca elements in SS. The composition and structure of SS were modified by this multi-component composite modifier. In this way, the secondary phase reaction was controlled, and the content of cementitious phase (C₃S, C₂S, and C₃A) and glass phase in SS was increased. The CMSFR helps to stabilize the unsoundness components in SS, and enhance the cementitious properties of SS, providing a reference for harmless application of SS and silicon-aluminum based solid waste in cement and concrete.

2 Materials and methods

2.1 Experimental materials

- (1) SS. This study uses converter SS without going through heat stewing from China Shougang Group Qian'an Steel Co., LTD. The SS meets the requirements in *Steel slag powder used for cement and concrete* (GB/T 20491-2017). According to Mason's (1944) formula $\text{CaO}/(\text{SiO}_2 + \text{P}_2\text{O}_5)$, the alkalinity of the SS is calculated as 2.79, its pH value is 12.1. Thus, the SS is highly alkaline. The f-CaO content in raw SS is 6.01%. The particle size analysis of the raw SS shows that 81.57% of the SS particles are distributed between 0.3 mm and 9.5 mm. Hence, the raw SS must be crushed before being ground. After processing, the specific surface area (SSA) of SS powder is 420 m² kg⁻¹. The activity indexes of raw SS for 7 days and 28 days are measured to be 63.4% and 71.1%, respectively, according to *Steel slag powder used for cement and concrete* (GB/T 20491-2017).

The raw SS powder is used as blank samples for comparative analysis with SMHTM, and marked as S0. The main minerals of raw SS include RO phase, C₃S, and C₂S (Figure 2A). In addition, the



heavy metal leaching toxicity of SS meets the requirements of Identification standards for hazardous wastes-Identification for extraction toxicity (GB 5085.3-2007) (Table 2).

(2) RS. The RS was taken from Yuecheng Reservoir in Handan, Hebei Province, China. The RS is fine particles with a small amount of water grass and other impurities. The surface color is gray. The water content is about 70%. After precipitation and dewatering, the RS was placed in a cool indoor place for air drying. Then, it was dried in a drying box (105°C). After that, the RS was crushed to less than 2 mm by roller pressing, and blended well. The blended sample was further dried at 105°C for 24 h. The dried sample was ground to -0.074 mm by an agate grinder, and sealed for further use.

According to the results of X-ray fluorescence analysis (XRF) (Table 1), the RS mainly encompasses inorganic substances and a small amount of organic matter (14.43%). The inorganic substances include Al_2O_3 (14.32%), SiO_2 (51.41%), $\text{Na}_2\text{O}+\text{K}_2\text{O}$ (2.58%), $\text{CaO}+\text{MgO}$ (7.54%), and $\text{Fe}_2\text{O}_3+\text{FeO}$ (7.30%). Therefore, the pyrolyzed RS must perform well in gas production. The heavy

metal contents (Cu, Zn, Pb, and Cd) in RS are lower than the limits in Identification standards for hazardous wastes-Identification for extraction toxicity (GB 5085.3-2007) (Table 2). As shown in Figure 2B, the main minerals in RS are berlinite, biotite, magnesium calcite, calcite, and quartz.

(3) SCS. The SCS was obtained from Inner Mongolia Power Generation Co., LTD., China Datang Group. The SCS is the waste produced by extracting aluminum from FA through limestone sintering. In the raw SCS, the water content is as high as 34.6%. Table 1 lists the chemical composition of the dried SCS. The alkali content ($\text{Na}_2\text{O}+0.658\text{K}_2\text{O}$) of 4.08% suggest that SCS is not suitable to be directly used as cement mixture and clinker. The main minerals of SCS include quartz, calcite, mullite, and C_2S (Figure 2C). The leaching toxicity of heavy metals in SCS meets the requirements of Identification standards for hazardous wastes-Identification for extraction toxicity (GB 5085.3-2007) (Table 2).

(4) FA. The FA was obtained from Inner Mongolia Power Generation Co., LTD., China Datang Group. Table 1 presents the main chemical composition of FA. Owing to the

TABLE 1 Chemical composition of raw materials (wt%).

Materials	SiO ₂	Al ₂ O ₃	CaO	MgO	Fe ₂ O ₃	FeO	Na ₂ O	K ₂ O	SO ₃	P ₂ O ₅	LOI
SS	11.11	4.89	35.89	8.33	23.58	6.32	0.48	0.13	0.26	1.74	2.72
RS	51.41	14.32	5.18	2.36	5.29	2.01	0.58	2.12	0.46	1.84	14.43
SCS	25.15	8.63	46.87	2.58	2.49	1.29	3.40	1.04	0.38	—	7.42
FA	42.22	40.89	4.73	0.77	3.77	0.11	0.26	0.53	0.59	0.28	3.95
Cement	22.50	4.86	66.30	0.83	3.43	0.21	0.24	0.31	—	0.02	0.12

TABLE 2 Leaching toxicity test results of raw materials (mg·L⁻¹).

Materials	Cu	Pb	Zn	Ni	Cd	Cr	As	Hg
SS	7.813	0.06	22.19	0.0166	0.2151	0.587	0.0022	—
RS	26.161	0.16	37.71	0.0110	0.0908	0.172	0.1116	0.00224
SCS	1.682	0.07	18.46	0.0246	0.1361	1.354	0.3791	0.02480
FA	0.923	0.03	15.32	0.0125	0.0624	0.0573	0.2581	—
Limit value	100	5	100	5	1	5	5	0.1

high content of Si and Al, the FA can be used as a Si-Al modifier. According to Fly ash used for cement and concrete (GB/T 1596-2017), a comprehensive analysis of the fineness, water demand ratio, loss, water content, and SO₃ mass fraction of FA shows that the FA used in the study belongs to Class C. The main mineral phases of FA are quartz, mullite, magnetite, and hematite, as shown in Figure 2D. The heavy metal leaching toxicity of FA meets the requirements in Identification standards for hazardous wastes-Identification for extraction toxicity (GB 5085.3-2007) (Table 2).

- (5) P·O 52.5 Portland cement. The cement is P·O 52.5 Portland cement produced by Jidong cement factory of BBMG Group, China. Whose chemical composition is displayed in Table 1. The initial and final setting time is 118 min and 190 min, respectively, which meet the requirements of Common Portland cement (GB 175-2007).

2.2 Experimental method

Based on the analysis of raw material characteristics, HTM of SS was carried out according to Figure 3. The cementitious properties and volume soundness of the MSM were investigated, and the reasons for the improvement of cementitious properties and soundness in SMHTM were analyzed in combination with the phase composition and structure. The following experimental methods were used in the study.

- (1) HTM test. Raw SS was obtained after drying, crushing, and ball milling, reaching a SSA of about 420 m² kg⁻¹. The three materials, namely, SCS, FA, and RS, were dried to constant weight. Then the SCS, FA and RS in CMFSR were mixed well in proportion and put into the ball mill and ground until the SSA was 440 m² kg⁻¹. Based on the research on modifiers used for

MSM by Zhang et al. (2012); Zhao et al. (2012), as well as the existing research foundation of the research group (Wang et al., 2022), according to the ratio of Ca, Si, and Al elements in SS, SCS, FA, and RS in Table 1, the ratio of SCS, FA, and RS in CMFSR is determined as 7:9:4. The pretreated SS powder was mixed with CMSFR in proportion. Table 3 illustrates the experimental scheme. The mixture was added an appropriate amount of water-based binder, and then evenly placed in a mold. Under a pressure of ≤30 MPa, the mixture was pressed into a φ 5 cm×3 cm cake. After that, the cake was relocated to a corundum crucible, and placed in a CD-1700X muffle oven for HTM. The modification temperature (MT) was set to 1,200°C, 1,250°C, and 1,300°C, and the heating rate was set to 10°C·min⁻¹. The temperature was held for 25 min after reaching each preset level. Then, the cake was taken out, and air cooled with a blower. Figure 3 shows the flow of SMHTM in laboratory.

- (2) Volume soundness test. The volume soundness test was conducted using the standards method in Test method for stability of steel slag (GB/T 24175-2009). The raw SS and MSM were finely ground in a ball mill and passed through a 200 mesh sieve to obtain a sample with a particle size less than 0.074 mm. The f-CaO content in the raw SS and MSM was determined by ethylene diamine tetra acetic acid (EDTA) complex metric titration. The sample of 0.8 g was placed in a 250 mL conical flask, 20 mL of 200 g L⁻¹ ethylene glycol solution was added and sealed with a cap, and the sample was kept at a constant temperature of 90°C for 3 min in a water bath. The solution was filtered through quantitative filter paper, and the filtrate was placed in a 250 mL conical flask with a little calcium indicator, and the calcium glycol in the solution to be measured was titrated with EDTA standard solution.
- (3) Heavy metal leaching test. SPLP was conducted to test the leaching behavior of heavy metals in raw materials, thus confirming the environmental safety. The methods of

leaching toxicity of heavy metals used the requirements of Identification standards for hazardous wastes-Identification for extraction toxicity (GB 5085.3-2007). During SPLP, the leach liquor was prepared by adding 60%/40% (mass fraction) of sulfuric acid/nitric acid and diluting appropriately with deionized water, in order to adjust the pH to 4.20 ± 0.05 (Wang et al., 2023a; Zhang et al., 2023). The leach liquor and solidified powder (0.075 mm) were mixed according to the ratio of 20:1, and shaken for 18 h in a gyrate shaker. Then, the screened mixture (0.45 μm) was put into Prodigy 7 Inductively coupled plasma emission spectrometer (ICP-OES) to analyze the concentration of Cr, Ni, Cu, Cd, Pb, Zn, As, and Hg (Wang et al., 2023b).

- (4) Mortar test of SS. The mortar test mainly investigates the cementitious activity of SS. Mortar blocks were prepared according to Method of testing cements-Determination of strength (GB/T17671-2021), using a 40 mm \times 40 mm \times 160 mm standard test mold. For the SS powder ground from mortar blocks, the SSA is 420 m² kg⁻¹, the water-cement ratio (W/C) is 0.5, and the cement-sand ratio (C/S) is 1:3. The mixing was carried out using a cement mortar mixer. Specifically, 1,350 g standard sand (C/S of 1:3) was added after 30 s low-speed stirring. When the stirring reached 60 s, the stirring mode was switched to 30 s high-speed stirring, 90 s stoppage, and 60 s high-speed stirring again. The mixed mortar paste was poured into the 40 mm \times 40 mm \times 160 mm standard test mold. Then, the test mold was placed on a vibration table for vibromolding. After that, the mortar paste was cured for 24 h under the standard conditions (temperature: $20 \pm 1^\circ\text{C}$; relative humidity $\geq 90\%$). Next, the test mold was removed, and the mortar block was relocated to a BWJ-III automated cement curing system at the temperature of $20 \pm 1^\circ\text{C}$. The strength of the mortar block was measured at the specified age. Compressive strength (CS): The average value of six CS measurements obtained from a group of three 40 mm \times 40 mm \times 160 mm is the test result. When one of the six measured values exceeds 10% of the average of the six, the result is rejected and the average of the remaining five is the result. When the five measured values exceed their average values by 10%, the group results are invalidated. When two or more of the six measured values exceed the average value by 10%, the results of this group are invalidated. Flexural strength (FS): a group of 40 mm \times 40 mm \times 160 mm flexural results of the average as the test results. When one of the three strength values exceeds the average value of 10%, should be removed and then take the average value as the test results of FS; when two of the three strength values exceed the average value of 10%, the remaining one as the result of FS.
- (5) SS activity index. The activity index of raw SS and SMHTM was determined according to Steel slag powder used for cement and concrete (GB/T 20491-2017):

$$A = \frac{R_t}{R_0} \times 100 \quad (1)$$

Where, A is the activity index of SS powder (%); R_t is the strength of the SS mortar block at the specified age (MPa); R_0 is the strength of the pure cement mortar block at the specified age (MPa).

- (6) SS paste test. The SS paste samples were prepared according to Test methods for water requirement of normal consistency, setting time and soundness of Portland cement (GB/T 1346-2011). Firstly, the stirring blade and stirring pot in the mixer were wiped clean with a wet mop. The SMHTM and water were added in proportion to the stirring pot. Then, the mixture was stirred at a low speed for 120 s, stopped for 15 s, and then stirred at a high speed for 120 s. The stirred paste was poured into a standard test mold of 20 mm \times 20 mm \times 20 mm for vibromolding. After that, the paste was cured for 24 h under the standard conditions (temperature: $20 \pm 1^\circ\text{C}$; relative humidity $\geq 90\%$). Next, the test mold was removed, and the paste sample was kept in a GB/T 17671-40A standard cement curing box. The standard curing continued until the preset age. The mechanical properties of the sample were measured at that age. After the SS paste test, the central part of the sample was taken, and soaked in anhydrous ethanol solution to stop hydration. Finally, the sample was dried for testing the composition and structure of the hydration products.

2.3 Property characterization

The particle size was analyzed with a Malvern 2000 laser particle size analyzer (range: 0.02–2,000.00 μm), with ethanol as dispersant. The particle size distribution was measured according to Particle size analysis-laser diffraction methods (GB/T 19077.1-2008). The SSA was measured by an SSA-3200 dynamic method SSA analyzer. The CS of samples at different ages was tested in reference to Method of testing cements-Determination of strength (GB/T 17671-2021). The mechanical properties of the samples were tested by a YES-300 digital hydraulic pressure testing machine (loading rate: (2.0 ± 0.5) kN/s; maximum load: 300 kN). The X-ray diffraction (XRD) was performed using a Rigaku D/MAX-RC 12 kW rotating anode diffractometer (Cu target; working current: 150 mA; working voltage: 40 kV; wavelength: 1.5406 nm). In addition, the scanning electronic microscopy (SEM) was implemented using an AMRAY1820 scanning electron microscope (resolution: 6nm; maximum magnification: 300,000 times; maximum acceleration voltage: 30 kV).

3 Results and discussion

3.1 Volume soundness of SMHTM

The HTM can promote the thermal-chemical reactions between f-CaO and SiO₂, Al₂O₃ in mineral admixtures. The reactions reduce the content of f-CaO, and increase the content of cement mineral phases in the SS. As a result, the air-cooled SS exhibits better cementitious activity and volume soundness. Using multi-component Si-Al solid waste, this paper prepares a CMSFR rich in Si-Al minerals, and reduces the f-CaO content in raw SS through the following high-temperature chemical equations:



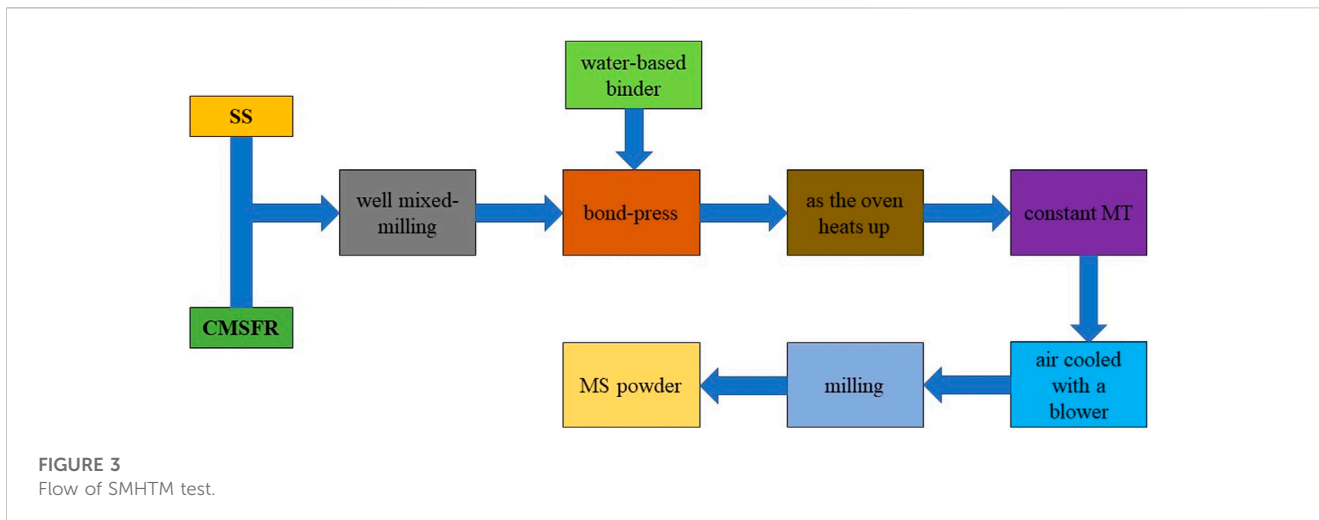


FIGURE 3 Flow of SMHTM test.

TABLE 3 Experiment scheme design of MSM.

Number	Mass fraction of mixture/%		Temperature (°C)
	S0	CMSFR	
S1	90	10	1,200
S2	80	20	
S3	70	30	
S4	90	10	1,250
S5	80	20	
S6	70	30	
S7	90	10	1,300
S8	80	20	
S9	70	30	

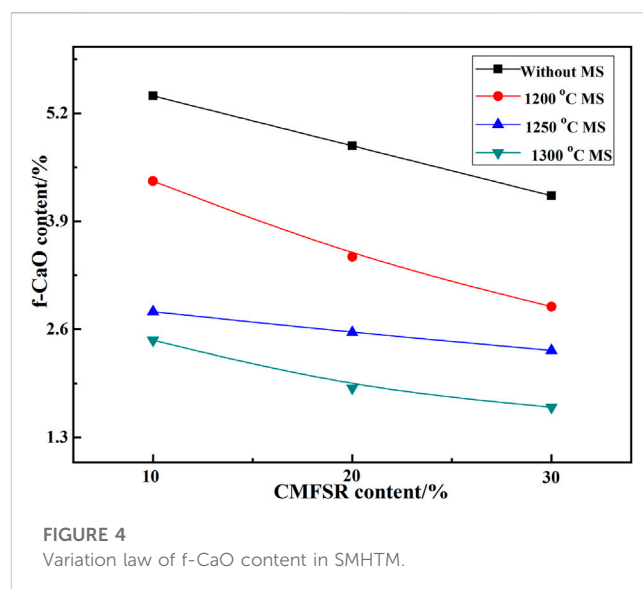


FIGURE 4 Variation law of f-CaO content in SMHTM.

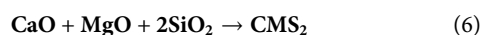
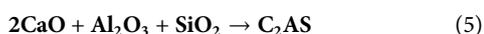


Figure 4 illustrates the changes in f-CaO content in SMHTM as a function of CMSFR content and MT. The raw SS of S0 and 10%–30% CMSFR mixed powder were selected as the comparison samples. As can be seen from Figure 4, the composite modifier CMSFR reduced the f-CaO content in the SS. The f-CaO content was greatly affected by MT and CMSFR content. The CMSFR content boosts MT, and suppresses f-CaO content in SMHTM.

At the CMSFR content of 10%, f-CaO content decreased from 4.38%, 2.81%–2.47%, as MT increased from 1,200°C, 1,250°C to 1,300°C. The f-CaO contents were 19.04%, 48.06%, and 54.34% smaller than those of the raw SS and CMSFR mixture, respectively. Similarly, at the CMSFR content of 20%, f-CaO content changed from 3.47%, 2.56%–1.90%, as MT rose from 1,200°C, 1,250°C to 1,300°C. The f-CaO contents were 28.48%, 46.78%, and 60.50% smaller than those of the raw SS and CMSFR mixture, respectively. At the CMSFR content of

30%, f-CaO content changed from 2.87%, 2.35%–1.66%, as MT rose from 1,200°C, 1,250°C to 1,300°C. The f-CaO contents were 31.83%, 44.18%, and 60.57% smaller than those of the raw SS and CMSFR mixture, respectively. Overall, when the MT was higher than 1,250°C and the CMSFR content was 10%–30%, the f-CaO content in the SMHTM remained below 3%, which meets the requirements in Steel slag powder used for cement and concrete (GB/T20491-2017).

The soundness of SS mainly comes from the volume expansion following f-CaO hydration. The SMHTM obtained with CMSFR can largely eliminate the volume unsoundness caused by f-CaO. Besides, SMHTM can be directly used in cement concrete, eliminating the need for aging treatment. The HTM boosts the thermochemical reactions between f-CaO and SiO₂, Al₂O₃, and other components in CMSFR, thereby reducing the f-CaO content in SS. However, after smelting at 1,650°C, the raw SS features dense structure, coarse grains, and solid melt RO phase. In this case, f-CaO cannot completely react with the chemical composition of CMSFR in SMHTM, resulting in incomplete removal of f-CaO.

TABLE 4 Properties and activity index of mortar samples with cement, S0 and SMHTM.

Group	Mortar fluidity/mm	Autoclave soundness	FS/MPa		CS/MPa		Activity index/%	
			7d	28d	7d	28d	7d	28d
C0	212	qualified	7.8	9.5	42.9	57.5	100.0	100.0
S0M	155	unqualified	5.1	7.2	27.2	40.9	63.4	71.1
SMHTM1	177	qualified	5.3	7.7	28.5	45.3	66.4	78.8
SMHTM2	188	qualified	5.7	8.3	30.9	46.1	72.0	82.2
SMHTM3	183	qualified	5.2	7.5	28.0	43.9	65.4	76.3
SMHTM4	207	qualified	5.8	8.4	31.2	47.8	72.7	83.1
SMHTM5	218	qualified	6.1	8.5	31.4	49.1	73.2	85.4
SMHTM6	197	qualified	5.6	8.2	30.8	46.7	71.8	81.2
SMHTM7	221	qualified	6.3	8.5	31.5	49.6	73.4	86.3
SMHTM8	227	qualified	6.4	8.6	31.9	50.9	74.4	88.6
SMHTM9	215	qualified	6.2	8.4	31.6	48.0	73.7	83.5

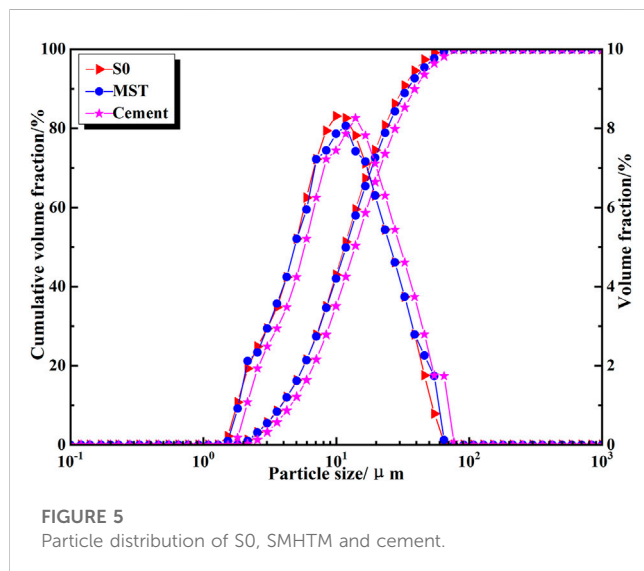


FIGURE 5 Particle distribution of S0, SMHTM and cement.

3.2 Cementitious properties of SMHTM

3.2.1 SMHTM activity

To investigate the cementitious properties of SMHTM, both the SMHTM and S0 particles were separately used as substitute for 30% (mass fraction) of P-O 52.5 cement. After mixing evenly, the properties and activity of each mortar sample were tested. The test results are recorded in Table 4, where C0 represents the mortar sample prepared with P-O 52.5 cement; S0M and SMHTM1 ~ SMHTM9 are the mortar samples prepared with 30% S0 and SMHTM, respectively. Figure 5 compares the particle size of S0, SMHTM powder, and cement. It can be observed that cement had a slightly lower particle content of 0.1–15 μm than S0 and SMHTM powder. As for the particle size >15 μm, cement had a higher particle content than SS powder, but the lead is very small.

As shown in Table 4, the mortar fluidity was small among S0M, SM 1 and SMHTM2, which may be attributed to the limited adaptability of S0 to the test cement. The mortar fluidity of the other samples was large. Thus, these SMHTM powders adapt well to the test cement.

It can be also seen from Table 4 that the mortar mixed with S0 had a low early strength. For this sample, the 7-day CS was 27.2 MPa, and 7-day activity index was 63.4%, a sign of improved later strength; the 28-day CS and activity index were 40.9 MPa, and 71.1%, respectively. For sample S0M, the 7-day FS and CS were 34.6% and 36.6% lower than those of pure cement mortar sample C0, respectively.

The CS and FS of mortars with SMHTM powders were better than those of S0M. Specifically, the 7-day FS increased by 2.0%–25.5%, and the 28-day FS increased by 4.2%–19.4%. Among all samples, SMHTM8 sample reached a 7-day FS of 6.4 MPa, and a 28-day FS of 8.6 MPa, which were 25.5% and 19.4% higher than those of sample S0M, respectively. The CS of mortar samples SMHTM1~SMHTM9, which were mixed with SMHTM powders, were 2.9%–17.3% and 7.3%–24.4% higher at 7 days and 28 days than those of S0M, respectively.

When CMSFR content was between 10% and 30%, the activity index of SS powder increased with MT. At the MT of 1,200°C and the CMSFR content of 10%–30%, the 28-day activity index of SMHTM powder increased by 5.2%–11.1% from the level of S0. At the CMSFR content of 20%, the 28-day activity index of SMHTM powder peaked at 82.2%. At the MT of 1,250°C and the CMSFR content of 10% and 20%, the 28-day activity index of SMHTM powder was 12.0% and 14.3% higher than that of S0 powder, respectively, and the activity index of SMHTM meets the requirement of Steel slag powder used for cement and concrete (GB/T 20491-2017): the activity index of grade I SS powder must be greater than or equal to 80%.

When the MT rose to 1,300°C and CMSFR content stood at 10% and 20%, the 28-day activity index of SMHTM powder were 86.3% and 88.6%, respectively, 15.2% and 17.5% higher than those of raw

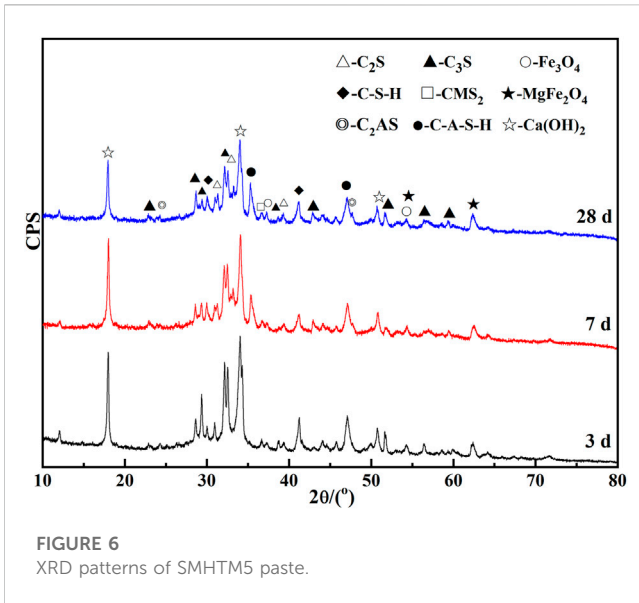


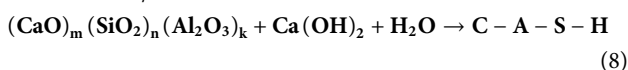
FIGURE 6
XRD patterns of SMHTM5 paste.

SS powder. Nevertheless, when CMSFR content grew to 30%, the cementitious activity of MSM at 1,250°C and 1,300°C were weaker than that of MSM at the CMSFR content of 20%. As shown in Table 4, adding 15%–25% CMSFR can effectively improve the cementitious properties of the system, when the MT is controlled at $\geq 1,250^\circ\text{C}$.

The FS and CS of SMHTM samples were lower than those of pure cement, which can be attributed to the reduced presence of cementitious phases C_3S , C_2S , and C_3A than P·O 52.5 cement. The HTM with CMSFR lays the basis for enhancing the cementitious activity of SS. The cementitious properties of the system can be effectively improved by preparing CMSFR out of cheap Si–Al waste, and improving the Ca/Si ratio of the system.

3.2.2 Composition and structure of hydration products of SMHTM

Figure 6 shows the XRD patterns of paste samples at different ages. These samples were prepared by SMHTM5, which was produced at the CMSFR content of 20% and the MT of 1,250°C. It can be found that, after 3 days, 7 days, and 28 days of hydration, the main products of the SMHTM5 paste samples include $\text{Ca}(\text{OH})_2$, C_2S , C_3S , unformed C–S–H gel, C–A–S–H, diopside ($\text{CaO}\cdot\text{MgO}\cdot 2\text{SiO}_2$, CMS_2), ceylonite ($\text{MgO}\cdot\text{Fe}_2\text{O}_3$, MgFe_2O_4), gehlenite ($2\text{CaO}\cdot\text{Al}_2\text{O}_3\cdot\text{SiO}_2$, C_2AS), and Fe_3O_4 . Among them, $\text{Ca}(\text{OH})_2$, C–S–H gel, and C–A–S–H are hydration products. The presence of C_2S and C_3S indicates that the SMHTM5 paste system is not completely hydrated (Singh and Vashistha, 2021). Similar to CC, the active minerals C_3S and C_2S in SMHTM are hydrated to form $\text{Ca}(\text{OH})_2$ and C–S–H gel (Eq. 7):



In addition, the steamed bread peak in the range of 25–40° (Figure 6) indicates the presence of amorphous vitreous body $((\text{CaO})_m (\text{SiO}_2)_n (\text{Al}_2\text{O}_3)_k)$ in SMHTM. The vitreous body

exhibits certain pozzolanic activity (Wilson et al., 2018; Mejdi et al., 2019) (see Eq. 8). $\text{Ca}(\text{OH})_2$, a hydration product of C_2S and C_3S in SMHTM, will be consumed by the glass phase, and the mineral content of C_2S and C_3S in MSM will affect the hydration rate, thereby altering the activity index of SMHTM and the CS of mortar samples. C_2AS minerals, mostly existing in the form of vitreous body, can react in an alkaline environment. The C_2AS in the product is the residue of the reaction (8). In fact, Eq. 8 also explains the appearance of C–A–S–H crystals in the hydration products. With the extension of curing age, the $\text{Ca}(\text{OH})_2$ generated by hydration of C_2S and C_3S reacted with amorphous vitreous continuously, which weakens the intensity of $\text{Ca}(\text{OH})_2$ diffraction.

Figure 7 shows the SEM images of SMHTM5 paste samples cured for 3 days, 7 days and 28 days. From Figures 7A, B, it can be found that large plate-like hydration product $\text{Ca}(\text{OH})_2$ crystals and loose honeycomb-like C–S–H gel appeared in the SMHTM5 paste sample at 3 days. Some $\text{Ca}(\text{OH})_2$ crystals are embedded in C–S–H gel. The structures were not highly compact or cementitious.

From Figures 7C, D, it can be found that, after 7-day curing, lots of thick C–S–H gel with thin two ends appeared in the middle, obeying a radiating distribution. Many 5–15 μm pores emerged in the upper right of Figure 7C. In addition, plate-like $\text{Ca}(\text{OH})_2$ crystals are seen in some parts of the visual range.

From Figures 7E, F, the C–S–H gel has a dense structure with sporadic pores at the age of 28 days. The number of pores has a significant decrease. There are 5–10 μm plate-like $\text{Ca}(\text{OH})_2$ crystals in the middle, which are much smaller than those in Figures 7A, B. The development law of hydration products in Figure 8 is basically consistent with the law of XRD in Figure 7.

3.3 Phase and structure of SMHTM

3.3.1 Phase composition of SMHTM

The phase composition of SMHTM was analyzed with the CMSFR content of 10%–30%, and the MT of 1,200°C–1,300°C (see Figure 8). Figure 8A presents the XRD patterns of MSM samples (SMHTM1, SMHTM4 and SMHTM7) at different MTs, when the CMSFR content was fixed at 10%. Figure 8B displays the XRD patterns of MSM samples (SMHTM4, SMHTM5 and SMHTM6) at the MT of 1,250°C and CMSFR content of 10%–30%.

The XRD pattern (Figure 2A) of the raw SS is referred for comparative analysis. In Figure 2A, the mineral compositions were RO phase, C_3S , C_2S , C_2F , f-CaO, C_{12}A_7 , and $\text{Ca}_2\text{Al}_2\text{Si}_3\text{O}_{12}$. The diffraction peaks of C_3S and C_2S were broad. After SMHTM was mixed with 10% CMSFR, the diffraction peaks of f-CaO became invisible (Figure 8). At the MT of 1,250°C, the diffraction peaks of C_3S and C_2S were significantly enhanced and sharpened. Therefore, the HTM promotes the formation of cementitious mineral phases. In cement production, 1,250°C is the commonly used temperature to regulate the formation of C_3S in the cementitious phase.

Comparing the curves of SMHTM1, SMHTM4 and SMHTM7 in Figure 8, it was learned that the C_3S of the cementitious phase was mainly concentrated in SMHTM4 (1,250°C), the diffraction peak of the C_3S mineral phase was relatively weak in SMHTM1 (1,200°C), and the C_3S diffraction peak was strong in SMHTM5. The air cooling (Figure 3) could effectively inhibit the decomposition of C_3S at a low temperature.

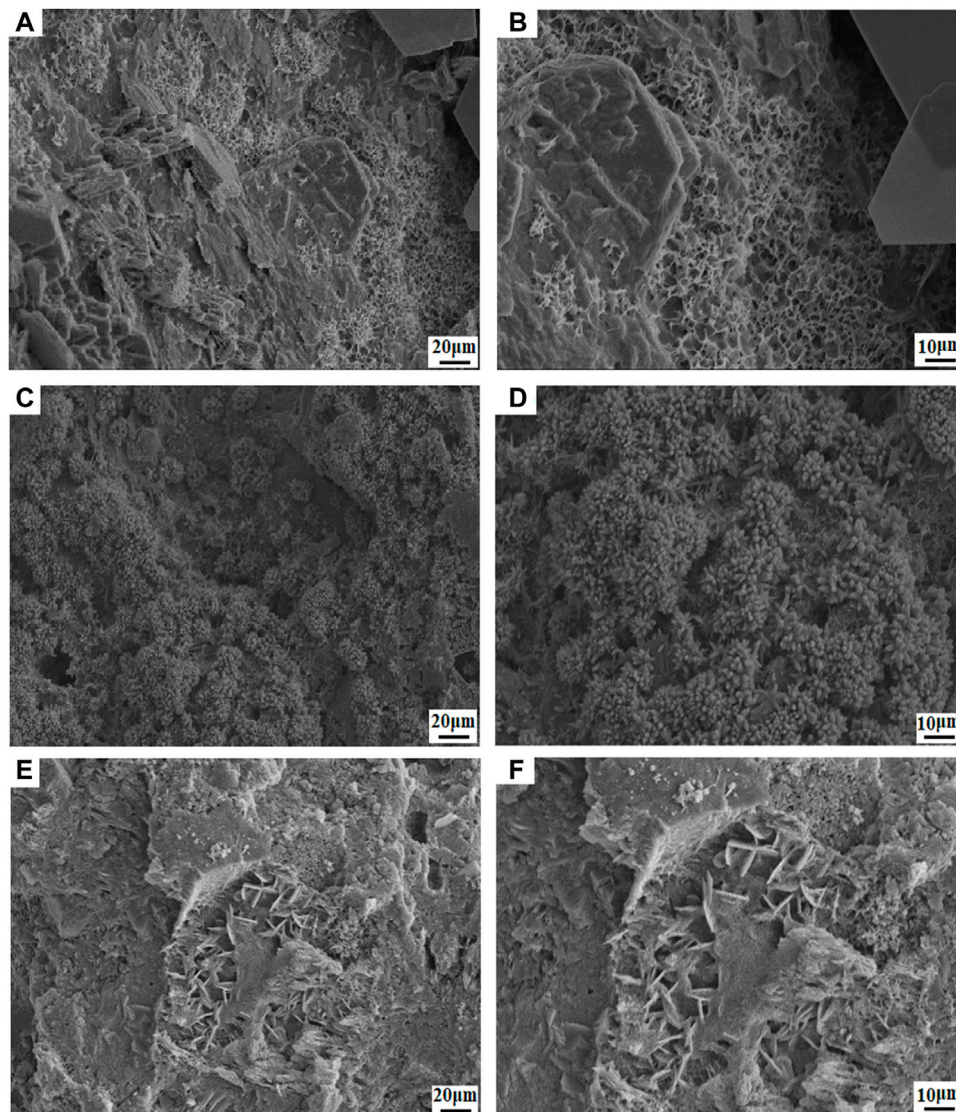


FIGURE 7
SEM images of SMHTM5 paste. (A, B)-3 days; (C, D)-7 days; (E, F)-28 days.

It can also be seen from [Figure 8](#) that the diffraction peak of RO phase in the STM was significantly weaker than that of the raw SS ([Figure 2A](#)). The solid-melt of the RO phase separates at high temperatures and undergoes thermochemical reactions with minerals in the CMSFR, turning the FeO in RO phase into MgFe_2O_4 and Fe_3O_4 . That is why the diffraction peak of Fe_3O_4 appears in [Figure 8](#), and widens with the growing temperature. There is no diffraction peak in the XRD pattern, because minerals other than C_2S in the raw materials of CMSFR, namely, SiO_2 , $3\text{Al}_2\text{O}_3 \cdot 2\text{SiO}_2$, CaCO_3 , $\text{CaMg}(\text{CO}_3)_2$, $\text{K}(\text{Mg,Fe})_3$, $\text{AlSi}_3\text{O}(\text{F,OH})$, and AlPO_4 participate in the modification reaction at a high temperature.

As shown in [Figure 8B](#), when the CMSFR content changed with the MT fixed to $1,250^\circ\text{C}$, the mineral phase composition in SMHTM varied significantly, mainly in the Si-Al-based mineral phase. When the content of CMSFR was 10%, the Si-Al-based minerals C_3S , C_2S ,

CMS_2 , C_2AS and C_3A were formed, in which C_3S , C_2S , C_3A , and C_2AS are cementitious phase. SMHTM had much more cementitious phase than the raw SS. The formation of CMS_2 , C_2AS , C_3A mineral phases is mainly due to the addition of CMSFR, and the decomposition of Al-containing components (C_{12}A_7 ($12\text{CaO} \cdot 7\text{Al}_2\text{O}_3$), $\text{Ca}_2\text{Al}_2\text{Si}_3\text{O}_{12}$) in the raw SS, which lowers the Ca/Si ratio in the system. After that, the liquid phase in the system increased under a high temperature, which promotes diffusion and crystal formation, as well as the formation of new mineral phases.

The analysis above indicates that, at the CMSFR content of 10–30% and the MT of $1,250^\circ\text{C}$, the content of cementitious phase was significantly increased in SMHTM, but the content of C_3S , C_2S and C_3A in the cementitious phase was lower than that in P-O 52.5 cement. As a result, the CS of the mortar sample obtained through the cementitious activity test on SS being

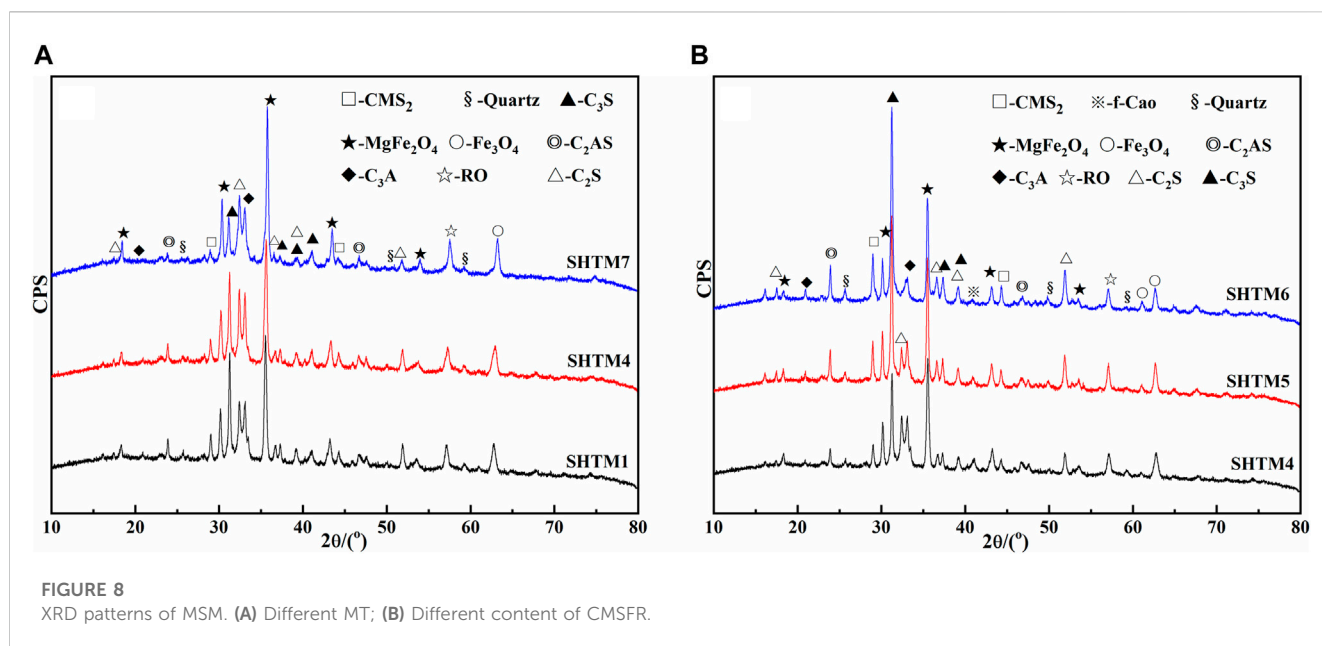
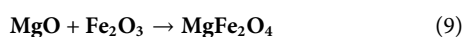


FIGURE 8
XRD patterns of MSM. (A) Different MT; (B) Different content of CMSFR.

inferior to that of the cement mortar sample. In our experiment, the CMSFR was prepared from FA, SCS, and RS. The HTM greatly elevates the content of C_3S and C_2S in the SMHTM, and produces new cementitious phases C_3A and C_2AS , offsetting the adverse effect of $f\text{-CaO}$ on the volume soundness of the raw SS. The reduction of RO phase content makes SS much more grindability. Combined with the XRD analysis on the mineral composition of the SMHTM, it is verified that the chemical reactions (Eqs 2–6) and (9) mainly occur during the SMHTM (Wang et al., 2022).



3.3.2 Microstructure of SMHTM

To further illustrate the role of CMSFR as a modifier, the authors analyzed the microstructure of SMHTM1, SMHTM5, and SMHTM9 at the MT of 1,200°C–1,300°C and the CMSFR content of 10%–30%, using SEM-EDS (see Figure 9).

From Figures 9A, 10, C_2AS (point 1) is the main matrix in SMHTM1 (10% CMSFR; 1,200°C) with the mineral particles being smooth. Most of them were triangular, and hexagonal, with small number were of prismatic minerals. The numerous produced minerals did not exhibit a specific distribution.

From Figures 9C, D, it was found that the C_2S with better crystallization grew concentratedly (point 2) on SMHTM5 (20% CMSFR; 1,250°C). The elliptical C_2S particles could reach more than 10 μm in size, and get closely combining with each other. The mineral particles had a smooth surface, clear boundaries, large SSA, and excellent cementitious activity. From Figures 9E, 10, it was found that $MgFe_2O_4$ is the main matrix in SMHTM (30% CMSFR; 1,300°C) (point 3). The crystal structure was quite regular, and relatively complete. The large crystal grains formed a tetrahedral stacking structure. The boundaries between them were quite obvious.

Figures 9G–I provides the EDS images of SMHTM at different MTs. Combining Figures 9A, B, it can be seen that the mineral surface in MSM was smooth, with no obvious boundaries. The proportion of Ca, Si and Al in the particles at point 1 was close to that of C_2AS . As a glass phase in SMHTM, C_2AS has low hydration activity under the excitation of alkaline solution. This again explains the lower activity index of SMHTM1 at 7 days and 28 days (66.4% and 78.8%).

The mineral crystal shape at point 2 in Figure 9D was well developed, obeying an elliptical grain distribution. The Ca/Si ratio was similar to that of C_2S (see Figure 9H). Due to air cooling, C_2S can stabilize in the $\beta\text{-}C_2S$ type, and witness a rise in hydration reactivity. That is why the activity indices of SMHTM5 samples at 7 days and 28 days were higher than those of SMHTM1.

The Ca/Si ratio at point 3 in Figure 9F was close to that of $MgFe_2O_4$ (see Figure 9I). The SS mixed with CMSFR produced a large amount of C_3S at 1,300°C. With the MgO from the RO phase gradually converting into $MgFe_2O_4$ as the temperature increases. The addition of CMSFR improves the Ca/Si ratio in the system. Under a high temperature, the amount of liquid phase increased, which facilitates diffusion and crystal production, and promotes the formation of C_3S . At the same time, the conditions were mature for the reaction of MgO and iron oxides to generate $MgFe_2O_4$. However, $MgFe_2O_4$ exists as an inert mineral in SMHTM, i.e., it does not undergo hydration reaction, resulting in a lower hydration rate of the material than Portland cement. Furthermore, the cementitious activity and activity index of SMHTM9 were lower than those of cement.

The combined analysis of the above studies shows that the results achieved in this study for MSM are better than those already reported by Zhang et al. (2012) and Zhao et al. (2012). In this study, the $f\text{-CaO}$ content of raw SS obviously decreased, and the cementitious properties improved in SMHTM. When the CMSFR content was 20% (SCS: FA: RS = 9:7:4), and the MT was 1,250°C,

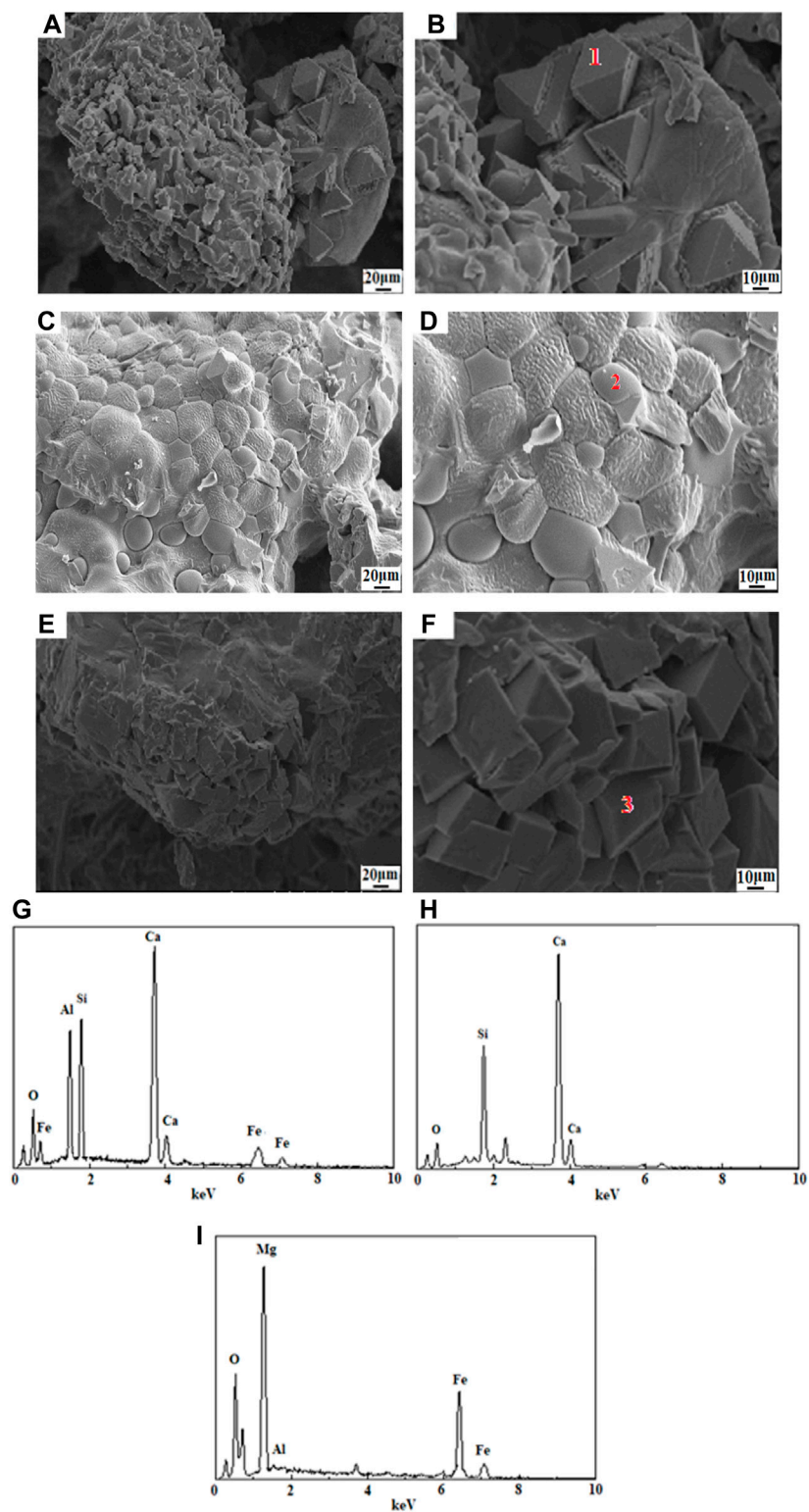


FIGURE 9
SEM-EDS images of SMHTM. (A, B)-SMHTM1; (C, D)-SMHTM5; (E, F)-SMHTM9; (G)-Point 1; (H) -Point 2; (I) -Point 3.

the mass fraction of f-CaO in SMHTM dropped from 4.81% to 1.90%, down by 60.5%; the 28-day activity index of SMHTM increased to 85.4%, 14.3% higher than that of raw SS, which

meets the technical requirement of Steel slag powder used for cement and concrete (GB/T 20491-2017): the activity index of grade I SS powder must be greater than or equal to 80%. However,



FIGURE 10
Cakes for HTM test.

in a study by Zhang et al. (2012) using iron ore tailings as a remodeling agent for reconstituted SS, when the treatment temperature was 1,250°C to 1,300°C and the iron ore tailing dosage was 10%–20%, the 28 days activity index of MSM increased from 76.4% to 83.4%, an increase of only 7.0%. According to Zhang et al. (2012) reported, the activity index of SMHTM at 1,300°C was 83.4%. However, in the author's study with 20% CMSFR added, the activity index of SMHTM at 1,250°C can reach 85.4%, and the activity index can reach 88.6% at 1,300°C, indicating that the energy consumption in Zhang's study is higher than that in the author's study. Similarly, the study of Zhao et al. (2012) used electric arc furnace (EAFSS) and FA as modifiers and the activity index of MSM was 85% when MT was 1,350°C. The energy consumption in his study was higher than that in this paper. From a comprehensive comparison perspective, the study in this paper is superior to the research of Zhang et al. (2012) and Zhao et al. (2012). The authors' study used SCS, FA and RS as modifiers, the presence of 14.43% organic matter in RS (Wang et al., 2022), and the residual carbon in FA can be effective in reducing MT.

4 Conclusion

Drawing on the idea of treating waste with waste, this paper prepares a composite modifier called CMSFR to improve the chemical and mineral composition of SS. The HTM with CMSFR improves the content of cementitious phase (C_3S , C_2S , C_3A) and glass phase in SS, and provides a reference for the harmless applications of SS and coal-based solid waste in cement concrete. The main conclusions are as follows.

- (1) SCS, FA and RS are cheap modification materials to realize HTM of SS. They can improve the cementitious activity of SS, and effectively reduce the content of f-CaO in SS. At the CMSFR content of 10%–30%, the 28-day activity index of raw SS increased by 17.5%, and the f-CaO content in SMHTM was minimized at 1.66%, meeting the requirement (f-CaO content $\leq 3\%$) in Steel slag powder used for cement and concrete (GB/T20491-2017).
- (2) The HTM changes the mineral composition of the raw SS, producing new cement phases like C_3A , C_2AS , and CMS_2 , $MgFe_2O_4$, and Fe_3O_4 . In addition, the f-CaO content decreased in the raw SS, while the content of C_3S and C_2S increased. The decomposition of $C_{12}A_7$ and $Ca_2Al_2Si_3O_{12}$ in raw SS promoted the formation of C_3A . During the HTM, the RO phase was decomposed, and the FeO in that phase was converted into Fe_3O_4 . The minerals other than C_2S in the raw materials of CMSFR participated in the HTM reactions.
- (3) At the MT of 1,200°C, the addition of 10% of CMSFR to the MSM produced C_2AS minerals in the shape of equilateral triangles, hexagons and a small number of prisms as the matrix. At the MT of 1,250°C, the addition of 20% of CMSFR to the MSM produced elliptical C_2S particles with good crystallinity; the size of these particles could reach more than 10 μm . At the MT of 1,300°C, the addition of 30% of CMSFR to the MSM generated $MgFe_2O_4$ minerals in the form of stacked regular tetrahedrons.

Data availability statement

The raw data supporting the conclusion of this article will be made available by the authors, without undue reservation.

Author contributions

DY proposes method and writes manuscript; CW proposes and participates in design research and reviews paper; XL, YG, HP, JM, YZ, JJ, YQ, YZ, and FL participate in design research and reviews paper. All authors contributed to the article and approved the submitted version.

Funding

The authors gratefully acknowledge financial support by the National Key Research and Development Program of China (No. 2021YFC1910605), the Natural Science Foundation of Hebei Province (E2020402079), State Key Laboratory of Solid Waste Resource Utilization and Energy Conservation (SWR-2023-007), Science and Technology Research and Development Plan of China Railway Construction Group Co., Ltd. (No. 22-11b, 22-14b), Handan Science and Technology Research and Development Program (21422111260). The funder was not involved in the study design, collection, analysis, interpretation of data, the writing of this article or the decision to submit it for publication.

Conflict of interest

YZ and FL were employed by China Railway Construction Group Co., Ltd.

The remaining authors declare that the research was conducted in the absence of any commercial or financial relationships that could be construed as a potential conflict of interest.

Publisher's note

All claims expressed in this article are solely those of the authors and do not necessarily represent those of their affiliated

organizations, or those of the publisher, the editors and the reviewers. Any product that may be evaluated in this article, or claim that may be made by its manufacturer, is not guaranteed or endorsed by the publisher.

References

- Adolfsson, D., Robinson, R., Engström, F., and Björkman, B. (2011). Influence of mineralogy on the hydraulic properties of ladle slag. *Cem. Concr. Res.* 41 (8), 865–871. doi:10.1016/j.cemconres.2011.04.003
- Alanyali, H., Cöl, M., Yilmaz, M., and Karagöz, Ş. (2009). Concrete produced by steel-making slag (basic oxygen furnace) addition in Portland cement. *Int. J. Appl. Ceram. Tec.* 6 (6), 736–748. doi:10.1111/j.1744-7402.2008.02317.x
- Aldeeky, H., and Hattamleh, O. A. (2017). Experimental study on the utilization of fine steel slag on stabilizing high plastic subgrade soil. *Adv. Civ. Eng.* 2017, 1–11. doi:10.1155/2017/9230279
- Anastasiou, E., Filikas, K. G., and Stefanidou, M. (2014). Utilization of fine recycled aggregates in concrete with fly ash and steel slag. *Constr. Build. Mater.* 50, 154–161. doi:10.1016/j.conbuildmat.2013.09.037
- Biskri, Y., Achoura, D., Chelghoum, N., and Mouret, M. (2017). Mechanical and durability characteristics of High Performance Concrete containing steel slag and crystallized slag as aggregates. *Constr. Build. Mater.* 150, 167–178. doi:10.1016/j.conbuildmat.2017.05.083
- Cao, L., Shen, W. G., Huang, J. Q., Yang, Y., Zhang, D., Huang, X. Q., et al. (2019). Process to utilize crushed steel slag in cement industry directly: Multi-phased clinker sintering technology. *J. Clean. Prod.* 217, 520–529. doi:10.1016/j.jclepro.2019.01.260
- Dai, S., Zhu, H. J., Zhang, D. R., Liu, Z. Q., Cheng, S. Y., and Zhao, J. X. (2022). Insights to compressive strength, impermeability and microstructure of micro-expansion steel slag cement under constraint conditions. *Constr. Build. Mater.* 326, 126540. doi:10.1016/j.conbuildmat.2022.126540
- Dhoble, Y., and Ahmed, S. (2018). Review on the innovative uses of steel slag for waste minimization. *J. Mater. Cycles. Waste.* 20, 1373–1382. doi:10.1007/s10163-018-0711-z
- Gu, X. Y., Yu, B., Dong, Q., and Deng, Y. F. (2018). Application of secondary steel slag in subgrade: Performance evaluation and enhancement. *J. Clean. Prod.* 181, 102–108. doi:10.1016/j.jclepro.2018.01.172
- Guo, J., Bao, Y., and Wang, M. (2009). Steel slag in China: Treatment, recycling, and management. *Waste Manage.* 29, 318–330. doi:10.1016/j.wasman.2018.04.045
- Guo, X. L., and Pan, X. J. (2018). Mechanical properties and mechanisms of fiber reinforced fly ash-steel slag based geopolymer mortar. *Constr. Build. Mater.* 179, 633–641. doi:10.1016/j.conbuildmat.2018.05.198
- Guo, X. L., and Xiong, G. Y. (2020). Resistance of fiber-reinforced fly ash-steel slag based geopolymer mortar to sulfate attack and drying-wetting cycles. *Constr. Build. Mater.* 269, 121326. doi:10.1016/j.conbuildmat.2020.121326
- Hasita, S., Rachan, R., Suddepong, A., Horpibulsuk, S., Arulrajah, A., Mohammadinia, A., et al. (2020a). Performance improvement of asphalt concretes using steel slag as a replacement material. *J. Mater. Civ. Eng.* 32 (8), 04020227. doi:10.1061/(ASCE)MT.1943-5533.0003306
- Hasita, S., Suddepong, A., Horpibulsuk, S., Samingthong, W., Arulrajah, A., and Chinkulkijniwat, A. (2020b). Properties of asphalt concrete using aggregates composed of limestone and steel slag blends. *J. Mater. Civ. Eng.* 32 (7), 06020007. doi:10.1061/(ASCE)MT.1943-5533.0003148
- Humbert, P. S., and Castro-Gomes, J. (2019). CO₂ activated steel slag-based materials: A review. *J. Clean. Prod.* 208, 448–457. doi:10.1016/j.jclepro.2018.10.058
- Huo, B. B., Li, B. L., Chen, C., and Zhang, Y. M. (2021). Surface etching and early age hydration mechanisms of steel slag powder with formic acid. *Constr. Build. Mater.* 280, 122500. doi:10.1016/j.conbuildmat.2021.122500
- Huo, B. B., Li, B. L., Huang, S. Y., Chen, C., Zhang, Y. M., and Banthia, N. (2020). Hydration and soundness properties of phosphoric acid modified steel slag powder. *Constr. Build. Mater.* 254, 119319. doi:10.1016/j.conbuildmat.2020.119319
- Iacobescu, R. I., Angelopoulos, G. N., Jones, P. T., Blanpain, B., and Pontikes, Y. (2015). Ladle metallurgy stainless steel slag as a raw material in ordinary Portland cement production: A possibility for industrial symbiosis. *J. Clean. Prod.* 112, 872–881. doi:10.1016/j.jclepro.2015.06.006
- Jiao, W. X., Sha, A. M., Liu, Z. Z., Li, W., Jiang, W., Qin, W., et al. (2020). Study on thermal properties of steel slag asphalt concrete for snow-melting pavement. *J. Clean. Prod.* 277, 123574. doi:10.1016/j.jclepro.2020.123574
- Khan, M. S. H., Castel, A., Akbarnezhad, A., Foster, S., and Smith, M. (2016). Utilisation of steel furnace slag coarse aggregate in a low calcium fly ash geopolymer concrete. *Cem. Concr. Res.* 89, 220–229. doi:10.1016/j.cemconres.2016.09.001
- Kourounis, S., Tsvilis, S., Tsakiridis, P. E., Papadimitriou, G. D., and Tsibouki, Z. (2007). Properties and hydration of blended cements with steelmaking slag. *Cem. Concr. Res.* 37 (6), 815–822. doi:10.1016/j.cemconres.2007.03.008
- Kriskova, L., Pontikes, Y., Cizer, Ö., Mertens, G., Veulemans, W., Geysen, D., et al. (2012). Effect of mechanical activation on the hydraulic properties of stainless steel slags. *Cem. Concr. Res.* 42 (6), 778–788. doi:10.1016/j.cemconres.2012.02.016
- Kriskova, L., Pontikes, Y., Pandelaers, L., Cizer, Ö., Jones, P. T., Balen, K. V., et al. (2013). Effect of high cooling rates on the mineralogy and hydraulic properties of stainless steel slags. *Metall. Mater. Trans. B* 44 (5), 1173–1184. doi:10.1007/s11663-013-9894-9
- Li, B. L., Wang, Y. H., Liang, Y., and Zhang, Y. M. (2019). Sulfate resistance and hydration products of steam cured steel slag blended cement mortar under dry-wet cycle. *J. Sustain. Cem.-based.* 8 (6), 353–366. doi:10.1080/21650373.2018.1564709
- Li, X. L., Li, K. X., Sun, Q., Liu, L., Yang, J. L., and Xue, H. W. (2021). Preparation of cemented oil shale residue-steel slag-ground granulated blast furnace slag backfill and its environmental impact. *Materials* 14 (8), 2052–2073. doi:10.3390/ma14082052
- Li, X., Yu, J., Wei, X., and Zhang, S. (2011). Structural characteristics and hydration kinetics of modified steel slag. *Cem. Concr. Comp.* 41 (3), 324–329. doi:10.1016/j.cemconres.2010.11.018
- Liu, J. Z., Yu, B., and Wang, Q. (2020). Application of steel slag in cement treated aggregate base course. *J. Clean. Prod.* 269, 121733. doi:10.1016/j.jclepro.2020.121733
- Liu, S. J., Hu, Q. Q., Zhao, F. Q., and Chu, X. M. (2014). Utilization of steel slag, iron tailings and fly ash as aggregates to prepare a polymer-modified waterproof mortar with a core-shell styrene-acrylic copolymer as the modifier. *Constr. Build. Mater.* 72, 15–22. doi:10.1016/j.conbuildmat.2014.09.016
- Liu, W. H., Li, H., Zhu, H. M., and Xu, P. J. (2020). The interfacial adhesion performance and mechanism of a modified asphalt-steel slag aggregate. *Materials* 13 (5), 1180–1192. doi:10.3390/ma13051180
- Luxán, M. P., Sotolongo, R., Dorrego, F., and Herrero, E. (2020). Characteristics of the slags produced in the fusion of scrap steel by electric arc furnace. *Cem. Concr. Res.* 30 (4), 517–519. doi:10.1016/S0008-8846(99)00253-7
- Mason, B. (1944). The constitution of some basic open-hearth slags. *J. Iron Steel Inst.* 1 (1), 69–80.
- Mejdi, M., Wilson, W., Saillio, M., Chaussadent, T., Divet, T., and Tagnit-Hamou, A. (2019). Investigating the pozzolanic reaction of post-consumption glass powder and the role of portlandite in the formation of sodium-rich C-S-H. *Cem. Concr. Res.* 123, 105790. doi:10.1016/j.cemconres.2019.105790
- Mo, L. W., Zhang, F., Deng, M., Jin, F., Al-Tabbaa, A., and Wang, A. G. (2017). Accelerated carbonation and performance of concrete made with steel slag as binding materials and aggregates. *Cem. Concr. Comp.* 83, 138–145. doi:10.1016/j.cemconcomp.2017.07.018
- Mo, L. W., Zhang, F., and Deng, M. (2016). Mechanical performance and microstructure of the calcium carbonate binders produced by carbonating steel slag paste under CO₂ curing. *Cem. Concr. Res.* 88, 217–226. doi:10.1016/j.cemconres.2016.05.013
- Monshi, A., and Asgarani, M. K. (1999). Producing Portland cement from iron and steel slags and limestone. *Cem. Concr. Res.* 29 (9), 1373–1377. doi:10.1016/S0008-8846(99)00028-9
- Murri, A. N., Rickard, W. D. A., Bignozzi, M. C., and Riessen, A. van. (2013). High temperature behaviour of ambient cured alkali-activated materials based on ladle slag. *Cem. Concr. Res.* 43 (1), 51–61. doi:10.1016/j.cemconres.2012.09.011
- Palankar, N., Shankar, A. U. R., and Mithun, B. M. (2016). Durability studies on eco-friendly concrete mixes incorporating steel slag as coarse aggregates. *J. Clean. Prod.* 129, 437–448. doi:10.1016/j.jclepro.2016.04.033
- Peng, C., and Huang, L. (2010). Carbon steel slag as cementitious material for self-consolidating concrete. *J. Zhejiang Univ.-sc. A* 11 (7), 488–494. doi:10.1631/jzus.A0900635
- Qian, G. R., Sun, D. D., Tay, J. H., Lai, Z. Y., and Xu, G. L. (2002). Autoclave properties of kirschsteinite-based steel slag. *Cem. Concr. Res.* 32 (9), 1377–1382. doi:10.1016/S0008-8846(02)00790-1
- Rashad, A. M. (2019). A synopsis manual about recycling steel slag as a cementitious material. *J. Mater. Res. Technol.* 8 (5), 4940–4955. doi:10.1016/j.jmrt.2019.06.038
- Roslan, H., Ismail, M., Abdul-Majid, Z., Ghoreishamiri, S., and Muhammad, B. (2016). Performance of steel slag and steel sludge in concrete. *Constr. Build. Mater.* 104, 16–24. doi:10.1016/j.conbuildmat.2015.12.008
- Salman, M., Cizer, Ö., Pontikes, Y., Snellings, R., Vandewalle, L., Blanpain, B., et al. (2015). Cementitious binders from activated stainless steel refining slag and the effect of alkali solutions. *J. Hazard. Mater.* 286, 211–219. doi:10.1016/j.jhazmat.2014.12.046

- Saly, F., Guo, L. P., Ma, R., Gu, C. P., and Sun, W. (2018). Properties of steel slag and stainless-steel slag as cement replacement materials: A comparative study. *J. Wuhan Univ. Technol.* 33 (6), 1444–1451. doi:10.1007/s11595-018-1989-3
- Saxena, S., and Tembhurkar, A. R. (2018). Impact of use of steel slag as coarse aggregate and wastewater on fresh and hardened properties of concrete. *Constr. Build. Mater.* 165, 126–137. doi:10.1016/j.conbuildmat.2018.01.030
- Shi, C. J., and Hu, S. F. (2003). Cementitious properties of ladle slag fines under autoclave curing conditions. *Cem. Concr. Res.* 33 (11), 1851–1856. doi:10.1016/S0008-8846(03)00211-4
- Shi, C. J. (2004). Steel slag—Its production, processing, characteristics, and cementitious properties. *J. Mater. Civ. Eng.* 16, 230–236. doi:10.1061/(ASCE)0899-1561(2004)16:3(230)
- Shi, C. (2004). Steel slag-its production, processing, characteristics and cementitious properties. *J. Mater. Civ. Eng.* 16 (3), 230–236. doi:10.1002/chin.200522249
- Shi, J. (2002). Characteristics and cementitious properties of ladle slag fines from steel production. *Cem. Concr. Res.* 2 (3), 459–462. doi:10.1016/S0008-8846(01)00707-4
- Singh, S. K., and Vashistha, P. J. (2021). Development of newer composite cement through mechano-chemical activation of steel slag. *Constr. Build. Mater.* 268, 121147. doi:10.1016/j.conbuildmat.2020.121147
- Tossavainen, M., Engstom, F., Yang, Q., Menad, N., Larsson, M. L., and Bjorkman, B. (2007). Characteristics of steel slag under different cooling conditions. *Waste Manage.* 27 (10), 1335–1344. doi:10.1016/j.wasman.2006.08.002
- Tu, T. A., Huan, T. G., Huynh, N. N. T., and Son, N. K. (2019). Characterization of carbonated steelmaking slag and its potential application in construction. *Vie. J. Sci. Technol.* 57 (3A), 61–68. doi:10.15625/2525-2518/57/3A/14078
- Wu, S. P., Xue, Y. J., Ye, Q. S., and Chen, Y. C. (2007). Utilization of steel slag as aggregates for stone mastic asphalt (SMA) mixtures. *Build. Environ.* 42 (7), 2580–2585. doi:10.1016/j.buildenv.2006.06.008
- Waligora, J., Bulteel, D., Degruilliers, P., Damidot, D., Potdevin, J. L., and Measson, M. (2010). Chemical and mineralogical characterizations of ladle converter steel slags: A multi-analytical techniques approach. *Mater. Charact.* 61 (1), 39–48. doi:10.1016/j.matchar.2009.10.004
- Wang, C. L., Jing, J. L., Qi, Y., Zhou, Y. X., Zhang, K. F., Zheng, Y. C., et al. (2023a). Basic characteristics and environmental impact of iron ore tailings. *Front. Earth Sci.* 11, 1181984. doi:10.3389/feart.2023.1181984
- Wang, C. L., Qi, Y., Jing, J. L., Ma, J. T., Zhou, Y. X., Ping, H. Y., et al. (2023b). Properties and microstructure of total tailings cemented paste backfill material containing mining and metallurgical solid waste. *Front. Earth Sci.* 11, 1181952. doi:10.3389/feart.2023.1181952
- Wang, C. L., Zhao, G. F., Wang, Y. B., Zhang, S. H., Zheng, Y. C., Huo, Z. K., et al. (2022). Study on the high-temperature modified steel slag using reservoir sediment and carbide slag. *Mater. Rep.* 36 (9), 21040178. doi:10.11896/cldb.21040178
- Wang, C. L., Zhao, G. F., Zheng, Y. C., Zhang, K. F., Ye, P. F., and Cui, X. W. (2019). Study on the preparation of high performance concrete using steel slag and iron ore tailings. *J. New Electr. Sys.* 22 (4), 217–223. doi:10.14447/jnmes.v22i4.a07
- Wang, Q., Wang, D. Q., and Zhuang, S. Y. (2017). The soundness of steel slag with different free CaO and MgO contents. *Constr. Build. Mater.* 151, 138–146. doi:10.1016/j.conbuildmat.2017.06.077
- Wang, Q., Yan, P. Y., and Feng, J. W. (2011). A discussion on improving hydration activity of steel slag by altering its mineral compositions. *J. Hazard. Mater.* 186 (2-3), 1070–1075. doi:10.1016/j.jhazmat.2010.11.109
- Wang, Q., Yang, J. W., and Yan, P. Y. (2013). Cementitious properties of super-fine steel slag. *Powder Technol.* 245, 35–39. doi:10.1016/j.powtec.2013.04.016
- Wang, S. G., Li, X. M., Ren, K. B., and Liu, C. H. (2020). Experimental research on steel slag stabilized soil and its application in subgrade engineering. *Geotech. Geol. Eng.* 38, 4603–4615. doi:10.1007/s10706-020-01313-6
- Wang, S., Wang, C., Wang, H., Liu, Z., Qian, W., Jin, C., et al. (2018). Study on cementitious properties and hydration characteristics of steel slag. *Pol. J. Environ. Stud.* 27 (1), 357–364. doi:10.15244/PJOES/74133
- Wilson, W., Sorelli, L., and Tagnit-Hamou, A. (2018). Unveiling micro-chemo-mechanical properties of C-(A)-S-H and other phases in blended-cement pastes. *Cem. Concr. Res.* 107, 317–336. doi:10.1016/j.cemconres.2018.02.010
- Xue, Y. J., Wu, S. P., Hou, H. B., and Zha, J. (2006). Experimental investigation of basic oxygen furnace slag used as aggregate in asphalt mixture. *J. Hazard. Mater.* 138 (2), 261–268. doi:10.1016/j.jhazmat.2006.02.073
- Yan, P. Y., Mi, G. G., and Wang, Q. (2014). A comparison of early hydration properties of cement-steel slag binder and cement-limestone powder binder. *J. Therm. Anal. Calorim.* 115 (1), 193–200. doi:10.1007/s10973-013-3360-4
- Yüksel, I. (2017). A review of steel slag usage in construction industry for sustainable development. *Environ. Dev. Sustain.* 19, 369–384. doi:10.1007/s10668-016-9759-x
- Zhang, H. Z., Qi, Y., Jing, J. L., Wang, C. L., Zhou, Y. X., Zhang, K. F., et al. (2023). Properties and environmental impact of building foundation pit backfilling materials containing iron and steel solid waste. *Front. Earth Sci.* 11, 1181974. doi:10.3389/feart.2023.1181974
- Zhang, M. G., Li, K. Q., Ni, W., Zhang, S. Q., Liu, Z. Y., Wang, K., et al. (2021). Preparation of mine backfilling from steel slag-based non-clinker combined with ultra-fine tailing. *Constr. Build. Mater.* 320, 126248. doi:10.1016/j.conbuildmat.2021.126248
- Zhang, T. S., Yu, Q. J., Wei, J. X., Li, J. X., and Zhang, P. P. (2011). Preparation of high performance blended cements and reclamation of iron concentrate from basic oxygen furnace steel slag. *Resour. Conserv. Recycl.* 56 (1), 48–55. doi:10.1016/j.resconrec.2011.09.003
- Zhang, Z. S., Lian, F., Liao, H. Q., Yang, Q., and Cao, W. B. (2012). Modifying the properties of steel slag by iron tailings at high temperature. *J. Univ. Sci. Technol. B* 34 (12), 1379–1384. doi:10.13374/j.issn1001-053x.2012.12.011
- Zhao, D. Q., Zhang, D., Shen, W. G., Huang, J. Q., Tang, X. C., Yang, Y., et al. (2022). Investigation on industrial trial production of multi-phased clinker with crude granular steel slag. *J. Clean. Prod.* 337, 130467. doi:10.1016/j.jclepro.2022.130467
- Zhao, H. J., Yu, Q. J., Wei, J. X., Li, J. X., and Zhong, G. (2012). Effect of composition and temperature on structure and early hydration activity of modified steel slag. *J. Build. Mater.* 15 (3), 399–405. doi:10.3969/j.issn.1007-9629.2012.03.021
- Zhao, Y. L., Wu, P. Q., Qiu, J. P., Guo, Z. B., Tian, Y. S., Sun, X. G., et al. (2022). Recycling hazardous steel slag after thermal treatment to produce a binder for cemented paste backfill. *Power Eng.* 395, 652–662. doi:10.1016/j.powtec.2021.10.008
- Zhuang, S. Y., and Wang, Q. (2021). Inhibition mechanisms of steel slag on the early-age hydration of cement. *Cem. Concr. Res.* 140, 106283. doi:10.1016/j.cemconres.2020.106283